

Estimation of Image Bias Field with Sparsity Constraints

Yuanjie Zheng

zheng.vision@gmail.com

James C. Gee

James.Gee@uphs.upenn.edu

Penn Image Computing and Science Laboratory (PICSL),
University of Pennsylvania School of Medicine, Philadelphia, PA, USA

Abstract

We propose a new scheme to estimate image bias field through introducing two sparsity constraints. One is that the bias-free image has concise representation with image gradients or coefficients of other image transformations. The other constraint is that model fit on the bias field should be as concise as possible. The new scheme enables adaptive specifications of the estimated bias field's smoothness, and results in extremely accurate solutions with more efficient optimization techniques, e.g. linear programming. These distinguish our approaches from many previous methods. Our techniques can be applied to intensity inhomogeneity correction of medical images, illumination and vignetting estimation of images captured by digital cameras.

1. Introduction

In image analysis, an image is a 2D/3D data obtained with certain imaging techniques, and expected to have a similar appearance to some physical properties of a series of objects—surfaces or inside structures of a subject. Three basic elements determine the appearance of an image: imaging technique, physical properties of the objects, and radiation. Imaging technique can be founded for example on a digital camera, an Magnetic Resonance Imaging (MRI) machine, or a Computed Tomography (CT) machine. Physical properties are associated with the surface reflectance function of an object when we are using a digital camera to take photos, or some special properties of bodily structures when we are visualizing body's internal structures with MRI or CT machines. Radiation enables the objects to be “seen” and refers to the illumination for imaging with a digital camera, magnetic field with MRI, or X-ray beam with CT.

As in many previous work, each image can be decomposed into several major components. The *first* component is an ideal image formed purely by the physical property of the objects (surfaces or body tissues). To be simple, we usu-

ally assume each object characterized by a uniform physical property. However, in practice it is not necessarily true considering the intra-object spatial variations of physical property. Then, this ideal image can be further decomposed into a piecewise constant “cartoon” image depicting the inter-object difference of physical property and a field formed by the intra-object spatial variations. The *second* component is called the bias field caused by the spatial variations of radiation. It appears as the intensity inhomogeneity in MRI or CT images [13], the illumination changes [11, 8] or vignetting effect [15, 14] in images from digital cameras. Bias field usually exhibits spatially smooth changes in many practical circumstances. The *third* component is image noise. Image bias field and image noise are treated as image artifacts and need to be accounted for.

The artifact of spatial variations of intensity/color caused by the bias field has been a challenge for many image analysis algorithms, including image segmentation, image registration, object tracking, object recognition, etc. For example, the assumption of piecewise constancy on an ideal image is widely used in image segmentation. However, due to the intensity variations introduced by the bias field, this assumption cannot be satisfied any more, and many segmentation algorithms will then become infeasible [13, 10, 15, 14, 11, 8].

When the bias field is spatially smooth, fitting a model (e.g. the multivariate polynomial model) for the bias field is powerful due to its robustness to image noise and is a significant class of methods in previous work of bias field estimation. However, as to be detailed in next section, most previous model-fitting methods of bias field estimation have several weaknesses. *First*, one or more than one parameters controlling the smoothness degree of the estimated bias field are required to be predefined, e.g. the order of the polynomial model. In practice, it is not always an easy task. *Second*, only a local optima can be obtained in the optimization process of estimating the model parameters and a good estimation is conditioned on a good initialization. *Third*, constraints on the value of the estimated bias field

are not easy to be enforced. For example, some papers explained the *a priori* knowledge that intensity inhomogeneity or vignetting effect [15, 14] take value in $[0, 1]$ or around 1. However, without value constraints, the estimation may be beyond this range. Most previous work just try to truncate the resulting values out of this expected range.

In this paper, we propose a new scheme to estimate the bias field given a single image by utilizing two sparsity constraints. The first constraint is on the ideal image in the sense that it has concise representations [5] with image gradients or coefficients of an image transform (e.g. Wavelet transformation). We specifically use the ℓ^1 norm of image gradient to measure the sparsity and it can be easily extended to other transformations. The second constraint is on the fit model of bias field in the sense that it is expected to be as concise as possible. We specifically use the multivariate polynomial model and its sparsity is measured by the ℓ^1 norm of the model parameters. However, it can be easily extended to other models. Based on this new scheme, we propose two techniques to estimate the bias field model, through solving a linear programming problem and a re-weighted least squares problem, respectively.

Our new scheme is capable of handling effectively the weaknesses of previous methods. Specifically, these two proposed techniques can both adaptively specify an optimal smoothness degree for the model fit on the bias field. For the method based on linear programming, a global optima can be obtained and constraints on the value of bias field can be easily added. Comprehensive experiments show that our techniques are more accurate and easier to use in practice.

2. Previous Work

A wide variety of methods have been proposed to estimate bias field in the research areas of intensity inhomogeneity correction of medical images [13, 10], illumination estimation [11, 8], and vignetting correction [15, 14]. There are many methods in each area that can also be used in other areas by some simple adjustments, considering the above explained similarities between the problems tackled in these areas. From the number of images needed by the estimation, the previous methods can be categorized into two classes: single image based and multiple images based. We below provide a brief review on single image based methods because it is the topic of this paper. Single image based methods can be further divided into two classes based on the reconstruction ways for the bias field: fit a predefined model of bias field based on different criteria, and identify intensity changes caused by the bias field (from intensity changes of the ideal image).

For the model fitting methods, different models and different optimization criteria have been tried in previous work. Models include B-spline [10], multivariate polynomial, and the model based on local smoothness [15], etc.

To fit the chosen model, the *first* criterion is founded directly on the assumption that the ideal image is piecewise constant. Although this assumption is not always true considering the intra-object spatial variations of physical property as explained in Sec. 1, a reasonable estimation can generally be obtained in practice. With this criterion, the chosen model is estimated by recursively performing segmentation, and bias field estimation & correction, with hoping that each segmented region is homogenous in the sense of intensity/color or texture. These methods rely on the extra segmentation process, and therefore need additional computations, and their accuracy of bias estimation is also determined by the segmentation precision. The *second* major criterion is based on the probability distribution of image intensities or gradients. The corresponding methods try to iteratively estimate the bias field model through maximizing high frequency of intensity histogram [10], minimizing entropy of intensity probability distribution, or increasing symmetry of gradient probability distribution [15].

There are a number of common weaknesses for the previous model-fitting methods. *First*, smoothness of the estimated bias field can not be specified adaptively and need to be pre-defined by specifying some parameter(s) of the model, e.g. the order of the polynomial model, or the distance between knots of a B-spline. *Second*, only a local optima can be obtained for the estimation of model and the obtained accuracy is conditioned on the initialization. *Third*, we may expect the estimated bias field value to be confined in a range, but the range constraints can not be enforced. For example, vignetting effect is assumed to take value in $[0, 1]$ in [15, 14], and the intensity inhomogeneity is expected to be around and close to 1 in [10]. Most previous methods just truncate the estimated value if it is out of the expected range.

For the methods of identifying intensity changes caused by bias field, there also exist various methods. The *first* significant class is based on low-pass filtering [13], with trying to remove sharp changes of the image and thus resulting in a smoothly changing bias field. Its difficulty lie in the specification of a threshold to differentiate the intensity changes between the ideal piecewise constant component and the bias field. The *second* major class of methods learn to differentiate the derivatives of the ideal image and bias field [11]. Although good estimations were shown, accuracy is significantly influenced by the similarity between the training samples and testing samples.

Bias field is pre-known to be smooth for most cases of previous work. When an appropriate model is available to depict the bias field, model fitting is usually preferred. It is because modelling fitting is more robust to noise and can better guarantee smoothness of the estimated bias field.

3. Problem Definition

Given an image Z , we assume that it is the product of the corresponding ideal image I and bias field B :

$$Z_i = I_i B_i, \quad \text{for } 1 \leq i \leq n_p, \quad (1)$$

where n_p is the total number of pixels in the image and i indexes the pixels. This assumption complies with many previous works [13, 15, 11].

The task of bias field estimation is to estimate B together with I in Eq. (1) given Z . It is obviously an ill-posed problem because the number of unknowns is double the number of equations. To make this problem well-posed, additional information is required. A common approach is to add constraints on B and I , as detailed in Sec. 2. Most constraints in previous work came from the assumptions that the ideal image is piecewise constant and the bias field is smooth. We will introduce two new constraints in Sec. 4 in order to enable more efficient optimization techniques to solve this problem as explained in Sec. 5.

Taking logarithm on both sides of Eq. (1), the multiplication becomes addition:

$$\mathcal{Z}_i = \mathcal{I}_i + \mathcal{B}_i, \quad \text{for } 1 \leq i \leq n_p. \quad (2)$$

This conversion can bring in many conveniences in our analysis as will be shown in Sec. 5.

Denote the constraints on \mathcal{I} and \mathcal{B} with $\mathcal{K}_I(\mathcal{I})$ and $\mathcal{K}_B(\mathcal{B})$, respectively, the estimation of \mathcal{B} can be expressed as the below minimization problem

$$\hat{\mathcal{B}} = \arg \min_{\mathcal{B}} (\mathcal{K}_I(\mathcal{I}) + \mathcal{K}_B(\mathcal{B})). \quad (3)$$

Note that many constraints that need to be maximized can be transferred to a minimization problem. With Eq. (2), Eq. (3) is re-written as

$$\hat{\mathcal{B}} = \arg \min_{\mathcal{B}} (\mathcal{K}_I(\mathcal{Z} - \mathcal{B}) + \lambda \mathcal{K}_B(\mathcal{B})). \quad (4)$$

where parameter λ balances these two constraints.

4. Sparsity Constraints

Most constraints enforced in the optimization process of previous papers are built upon certain *a priori* knowledge on the ideal image \mathcal{I} or bias field \mathcal{B} . They make the estimated bias field as consistent as possible with the *a priori* knowledge. We below introduce two new sparsity constraints on \mathcal{I} and \mathcal{B} , respectively.

The ideal image is sparse in the sense of transform sparsity [5], i.e. \mathcal{I} has concise representations with transform coefficients from an orthogonal basis (e.g. a Fourier basis), tight frames (e.g. curvelet), or even image gradient [4]. Just with a small subset of these transform coefficients, \mathcal{I} can be

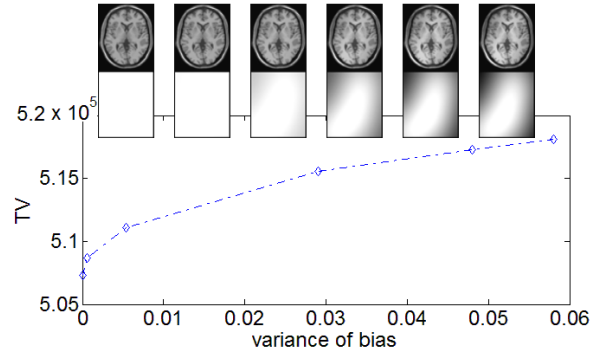


Figure 1. TV values of an MRI brain image with bias fields in different significance degrees (measured by the variance of the bias field). Each of the six brain images is created by adding the corresponding below bias field to an image free from bias artifact. From left to right, the simulated bias fields have increasing variances, and correspond to the six diamonds on the curve, respectively. The left most simulated field has zero bias effect.

reconstructed very well. It is true for most piecewise constant images as shown in many existing papers on sparse representation of image.

The smooth bias field is sparse in the sense that \mathcal{B} can be represented by a model as concisely as possible. Specifically, \mathcal{B} can be represented precisely by a model with a very small number of nonzero parameters for models like the polynomial model or a very small value diversity of parameters for models like B-spline.

4.1. Sparsity of Piecewise Constant Image

In a piecewise constant image, the number of jumps (discontinuities) is much smaller than the number of pixels. There are different sparsity measures for a piecewise constant image \mathcal{I} : the ℓ^0 norm [6] or the ℓ^p ($0 < p < 2$) norm [5, 12] of the transformation coefficients of orthogonal basis or tight frames, the ℓ^1 norm of the magnitudes of the image discrete gradient, i.e. the total variation (TV) [4], etc. We choose TV and extension to other measures is trivial. TV is computed as the ℓ^1 norm of the image gradients:

$$TV(\mathcal{I}) = \|\nabla \mathcal{I}\|_{\ell^1} = \sum_i |\nabla \mathcal{I}_i| \quad (5)$$

where $\nabla \mathcal{I}_i$ means the gradients of \mathcal{I} at pixel i . $\nabla \mathcal{I}_i$ is a vector composed by gradients at different directions (e.g. x and y for a 2D image, x , y , and z for a 3D volume data). $\nabla \mathcal{I}$ denotes a vector concatenated by $\{\nabla \mathcal{I}_i\}$.

Generally speaking, a more significant bias field artifact makes the TV value of the image larger, as shown by Fig. 1. In this figure, the bias fields are simulated by differently scaling a simulated field created with the polynomial model explained in next section.

4.2. Sparsity of Bias Field

We try to fit a model on the bias field with expecting that the model is as concise as possible. It is because of the *a priori* known spatial smoothness of the bias field. The model is estimated by minimizing/maximizing some sparsity measures. As talked above, different models may have different definition of sparsity measure.

We choose the multivariate polynomial model. For a 2D image and in degree D , it is expressed as

$$\mathcal{B}_i = \sum_{t=0}^D \sum_{l=0}^{D-t} a_{t,l} x_i^t y_i^l \quad (6)$$

where $\{a_{t,l}\}$ are model parameters, and x_i and y_j are coordinates of pixel i . Note that the number of elements in $\{a_{t,l}\}$ is $n_a = (D+1)(D+2)/2$. We can concatenate $\{a_{t,l}\}$ to create a vertical vector denoted by \mathbf{a} .

A smoother bias field can generally be represented accurately by a polynomial model in a lower degree (as shown by Fig. 3), i.e. with fewer parameters $\{a_{t,l}\}$. An obvious measure on the sparsity of \mathcal{B} is the number of nonzero elements in \mathbf{a} , calculated by the ℓ^0 norm:

$$\|\mathbf{a}\|_{\ell^0} = \#\{(t,l) : a_{t,l} \neq 0\} \quad (7)$$

where $\#$ means the number of elements in a set. For a smooth bias field, if we instead use a polynomial model of very high degree, the value of $a_{t,l}$ corresponding to large $\{t,l\}$ values should be zero.

However, optimizing an ℓ^0 norm in Eq. (7) is infeasible because a small perturbation on \mathbf{a} may change $\|\mathbf{a}\|_{\ell^0}$ significantly. A minimization problem involving an ℓ^0 norm is non-convex and hard to solve. Fortunately, as shown in [3], ℓ^1 norm is a good proxy for the ℓ^0 sparsity count and at the same time enables the problem to be convex. The ℓ^1 norm is computed as

$$\|\mathbf{a}\|_{\ell^1} = \sum_{(t,l)} |a_{t,l}|. \quad (8)$$

Given a different model such as the cubic B-spline, \mathcal{B} is sparse when the knots take values in a very small diversity, i.e. neighboring knots having very similar values. Therefore, bias field's sparsity can be measured by the ℓ^1 norm of the value differences between neighboring knots.

5. Solving Bias Field

5.1. Reformulation

Treating TV in Eq. (5) and ℓ^1 norm in Eq. (8) as the constraints \mathcal{K}_I and \mathcal{K}_B , respectively, Eq. (4) is rewritten as

$$\hat{\mathcal{B}} = \arg \min_{\{a_{t,l}\}} (\|\nabla \mathcal{Z} - \nabla \mathcal{B}\|_{\ell^1} + \lambda \|\mathbf{a}\|_{\ell^1}). \quad (9)$$

where $\nabla \mathcal{Z}$ and $\nabla \mathcal{B}$ represents the vectors concatenated by $\{\nabla \mathcal{Z}_i\}$ and $\{\nabla \mathcal{B}_i\}$, respectively. Obviously, the lengths of $\nabla \mathcal{Z}$ and $\nabla \mathcal{B}$ are both equal to $2n_p$ for a 2D image.

In Eq. (9), $\nabla \mathcal{Z}$ is known and can be obtained directly from the given image. For $\nabla \mathcal{B}$, each element can be expressed as a linear combination of model parameters \mathbf{a} . Taking x component of $\nabla \mathcal{B}_i$ for example, from Eq. (6), we have the expression

$$\psi_x^{\mathcal{B}}(i) = \frac{\mathcal{B}_i - \mathcal{B}_{i'}}{\delta x} = \frac{1}{\delta x} \sum_{t=0}^D \sum_{l=0}^{D-t} a_{t,l} (x_i^t - x_{i'}^t) y_i^l \quad (10)$$

where δx is the horizontal resolution of the given image, and i' is the left neighbor pixel of i . Obviously, $\psi_x^{\mathcal{B}}(i)$ can be reformulated as a linear combination format:

$$\psi_x^{\mathcal{B}}(i) = \mathbf{c}_{x,i}^T \mathbf{a} \quad (11)$$

where the components in $\mathbf{c}_{x,i}$ are the linear combination coefficients. We omit the expression of $\mathbf{c}_{x,i}$, which can be obtained easily from Eq. (10).

With Eq. (11), $\nabla \mathcal{B}$ in Eq. (9) can be rewritten as a multiplication of a constant matrix \mathbf{C} and the vector \mathbf{a} . Matrix \mathbf{C} is formulated by treating the transpose of each $\mathbf{c}_{x,i}$ in Eq. (11) as one of its rows. For each pixel and each direction of gradient, there exist a combination coefficient vector like $\mathbf{c}_{x,i}$. For a 2D image, the total number of this kind of vectors is $2N$. Therefore, the number of rows in \mathbf{C} is $n_{\nabla \mathcal{Z}}$ (the length of $\nabla \mathcal{Z}$) and the number of columns equals to n_a (the length of vector \mathbf{a}). We have the rewriting of $\nabla \mathcal{B}$:

$$\nabla \mathcal{B} = \mathbf{C} \mathbf{a}, \quad (12)$$

and then the rewriting of Eq. (9):

$$\hat{\mathcal{B}} = \arg \min_{\mathbf{a}} (\|\nabla \mathcal{Z} - \mathbf{C} \mathbf{a}\|_{\ell^1} + \lambda \|\mathbf{a}\|_{\ell^1}). \quad (13)$$

Eq. (13) can be further simplified by merging the second term into the first one. We first use \mathbf{I} to denote an identity matrix of size equal to n_a , and then create a new matrix

$$\mathbf{C}' = \begin{bmatrix} \mathbf{C} \\ \lambda \mathbf{I} \end{bmatrix}. \quad (14)$$

The numbers of rows and columns of \mathbf{C}' are $n_{\nabla \mathcal{Z}} + n_a$ and n_a , respectively. Obviously, matrix \mathbf{C}' is full rank. We then use $\mathbf{0} \in \mathbf{R}^{n_a}$ to denote a null vector, and rebuild $\nabla \mathcal{Z}$ as

$$\nabla \mathcal{Z}' = \begin{bmatrix} \nabla \mathcal{Z} \\ \mathbf{0} \end{bmatrix}, \quad (15)$$

where the length of $\nabla \mathcal{Z}'$ satisfies $n_{\nabla \mathcal{Z}'} = n_{\nabla \mathcal{Z}} + n_a$. We can now simplify Eq. (13) as

$$\hat{\mathcal{B}} = \arg \min_{\mathbf{a}} \|\nabla \mathcal{Z}' - \mathbf{C}' \mathbf{a}\|_{\ell^1}. \quad (16)$$

In some cases, we may also expect the estimation of bias field to be confined in a range, as expressed below

$$\mathcal{B}_l \leq \mathbf{C}' \mathbf{a} \leq \mathcal{B}_u. \quad (17)$$

where $\mathcal{B}_l, \mathcal{B}_u$ are the lower and upper bounds, respectively.

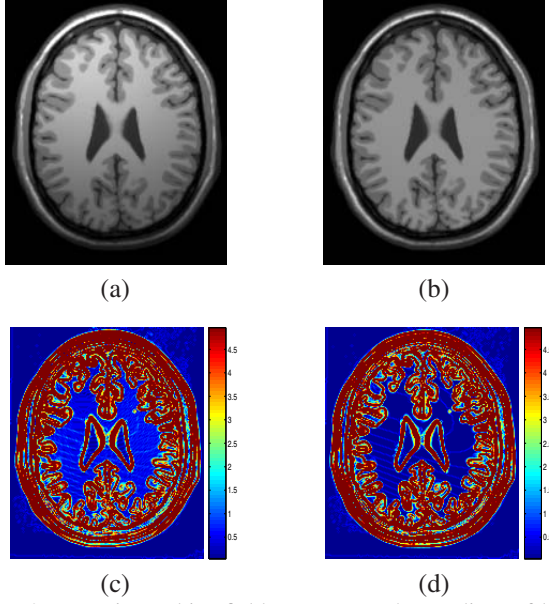


Figure 2. To estimate bias field, we expect the gradient of bias-corrected image is as sparse as possible. (a) MRI brain image with bias artifact. (b) Image after bias correction. (c) Gradient magnitude of (a). (d) Gradient magnitude of (b). Apparently, (d) is sparser (i.e. bearing fewer nonzero value) than (c) especially in the regions of white matter.

5.2. Solution

Given $\nabla Z'$, Eq. (16) finds the vector \mathbf{a} such that the residual $\nabla Z' - \mathbf{C}'\mathbf{a}$ has minimum ℓ^1 norm, i.e. we are expecting that the difference between $\nabla Z'$ and $\mathbf{C}'\mathbf{a}$ to be sparse. In other words, we hope that the gradient difference between the input image and the reconstructed bias field is sparse as shown in Fig. 2, and the estimated parameters of the bias field model are sparse.

We below provide two techniques for solving Eq. (16). They perform by solving a linear programming problem and a problem of re-weighted least squares, respectively.

5.2.1 Linear Programming

As in many existing papers using the linear programming techniques [1], Eq. (16) can be equivalently reformulated as a conditioned minimization problem as show below:

$$\min \mathbf{1}^T \mathbf{f}, \text{ subject to } \mathbf{f} \geq \mathbf{0} \text{ and } -\mathbf{f} \leq \nabla Z' - \mathbf{C}'\mathbf{a} \leq \mathbf{f} \quad (18)$$

where $\mathbf{1} \in \mathbf{R}^{n_{\nabla Z'}}$ is a vector of ones, and $\mathbf{f} \in \mathbf{R}^{n_{\nabla Z'}}$ is the vector of the auxiliary variables.

In Eq. (18), the vector inequality means enumerating the inequality between each element in one vector and the corresponding element in the other one. Eq. (16) is very similar to the problem of channel coding [2] where it was shown

that solving the linear programming problem in Eq. (18) can efficiently find an optimal solution for Eq. (16).

It now becomes trivial to provide the linear program:

$$\min \begin{bmatrix} \mathbf{1} \\ \mathbf{0} \end{bmatrix}^T \begin{bmatrix} \mathbf{f} \\ \mathbf{a} \end{bmatrix}, \text{ subject to } \begin{bmatrix} -\mathbf{I} & \mathbf{0} \\ \mathbf{0} & \mathbf{C}' \end{bmatrix} \begin{bmatrix} \mathbf{f} \\ \mathbf{a} \end{bmatrix} \leq \nabla Z', \quad (19) \\ \begin{bmatrix} \mathbf{I} & \mathbf{0} \\ \mathbf{0} & \mathbf{C}' \end{bmatrix} \begin{bmatrix} \mathbf{f} \\ \mathbf{a} \end{bmatrix} \leq \nabla Z', \\ -\mathbf{f} \leq \mathbf{0},$$

where the sizes of the identity matrix \mathbf{I} and all zero matrices denoted by $\mathbf{0}$ are specified to fit the variable vector $[\mathbf{f}^T \mathbf{a}^T]^T$.

The range constraints on \mathcal{B} in Eq. (17) can be incorporated in the linear program of Eq. (19) by the re-writings:

$$\begin{aligned} \mathbf{C}'\mathbf{a} &\leq \mathcal{B}_u \\ -\mathbf{C}'\mathbf{a} &\leq -\mathcal{B}_l \end{aligned} \quad (20)$$

To solve the linear programming problem expressed by Eq. (19) with Eq. (20), various solvers are available online. In our experiments, we use the interior point solver of the GNU Linear Programming Kit (GLPK)¹.

Treating Eq. (16) as a linear program has multiple advantages. First, the solution is accurate due to the power of convex optimization in linear programming. Second, range constraints can be easily added on the solution, as shown in Eq. (20). Third, implementation is easy with the online available linear programming solvers and new solvers with better performances can be directly incorporated.

However, a major limitation of solving a linear programming is the slow speed, due to the huge number of variables in \mathbf{f} . This can be handled by the other optimizing technique shown below, but with sacrificing accuracy in some degree.

5.2.2 Re-weighted Least Squares

Without considering the range constraints on \mathcal{B} in Eq. (17), Eq. (16) can also be reformulated as an iteratively re-weighted least squares (IRLS) problem [9]. IRLS poses the optimization as a sequence of standard least squares problems, each using a weight factor based on the solution of the previous iteration.

Specifically, at the k th iteration, the following minimization problem is to be solved:

$$\arg \min_{\mathbf{a}} \|\mathbf{W}\nabla Z' - \mathbf{W}\mathbf{C}'\mathbf{a}\|_{\ell^2} + \epsilon \|\mathbf{a}\|_{\ell^2} \quad (21)$$

where \mathbf{W} is a $n_{\nabla Z'} \times n_{\nabla Z'}$ diagonal matrix specifying the weight value on each component of $\nabla Z'$ and $\mathbf{C}'\mathbf{a}$. The second term of Eq. (21) is the regularization, giving preference to a solution of \mathbf{a} with smaller norms. Parameter ϵ is an adjusting parameter taking a small value (e.g. 0.0001). As a

¹<http://www.gnu.org/software/glpk/>

standard regularized least squares problem, Eq. (21) can be solved by the ridge regression technique [7]. We note that Eq. (21) can also be solved efficiently if the ℓ^2 norm of \mathbf{a} is replaced with ℓ^1 norm to get a sparse solution of \mathbf{a} , based on some recent work on sparse reconstruction [5].

Taking the i th diagonal element of \mathbf{W} for example, the weight is updated at the k th iteration as below

$$\mathbf{W}(i) = \exp^{-S_1(1 - \exp^{-S_2})}, \text{ for which} \\ S_1 = |\nabla Z'(i) - \mathbf{C}'\hat{\mathbf{a}}_{k-1}(i)|, \quad S_2 = \alpha (S_1)^{\alpha-1}, \quad (22)$$

where $\hat{\mathbf{a}}_{k-1}$ is the estimation of \mathbf{a} at the $(k-1)$ th iteration, and “ (i) ” is the i th element of the vector before it, and setting the adjusting parameter $\alpha = 0.7$ can always produce good weight values.

The IRLS process needs an initialization. We can simply set $a_{0,0} = 1$ and other parameters to be zero for the multivariate polynomial model in Eq. (6) (i.e. no bias), and set all weight values to be 1.

Compared with the linear programming technique, IRLS is pretty fast. A good estimation can be obtained by repeating the minimization in Eq. (21) for at most four times. However, the solution of IRLS is less optimal because it is a local minimum. In addition, the range constrains in Eq. (17) can not be incorporated.

6. Results and Discussions

A significant advantage of the two novel proposed techniques for estimating image bias field is their ability to adaptively determine the smoothness degree for the estimated bias field. For most previous methods not having this property, the bias effect may be under-estimated or over-estimated if the smoothness degree can not be guessed correctly by the user. Under-estimation happens when the smoothness is over-estimated by the user, i.e. a too small degree value is set for the polynomial model in Eq. (6). Running an algorithm on an image corrected with an under-estimated bias field, we can get another estimation in which the bias effect can be seen. Over-estimation takes place when the smoothness is under-estimated by the user, i.e. a too large degree value is set for the polynomial model in Eq. (6). In an over-estimated bias field, we may see brain (or other object) structure. The two awkward situations both mean that the estimation of bias field is erroneous.

Through our experiments, we find that the performances of our techniques are pretty robust to λ in Eq. (9) and D in Eq. (6). Accurate estimation can be produced when λ takes value in a large range, e.g. $0.5 \sim 10$ for which we have tested, and when D is large enough to be able to represent most bias fields in the data sets. In all the following experiments, we set $\lambda = 2$ and $D = 10$.

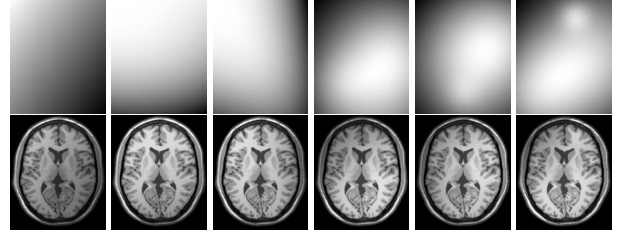


Figure 3. Upper: from left to right, six bias fields simulated with the polynomial model in Eq. (6) with degree values from 1 to 6. Lower: images formed by adding the upper bias fields to a bias-free brain image.

6.1. With Simulated Data

We compare the accuracies of our approaches with N3 [10] using a simulated brain image and multiple simulated bias fields. We choose N3 because it is one of the most widely used and standard approaches for bias correction in MRI brain images. For the test data, we download the bias-free simulated brain data on the BrainWeb¹. From this volumetric data, we choose one slice containing major anatomy structures of the brain as the test image.

To compare with N3, we first replace the B-spline model in N3 with the polynomial model in Eq. (6). Therefore, all methods in comparison have a uniform model and the errors caused due to model difference can be eliminated. We then simulate a series of 2D bias fields using the polynomial model in Eq. (6) with degree values from 1 to 6, respectively. The parameters $\{a_{t,l}\}$ are set as a random value between $[0 \ 1]$, and the resulting bias fields are then scaled to $[0.5 \ 1.5]$. The six simulated bias fields and the images obtained by adding these fields to the simulated brain image are shown in Fig. 3.

We perform two types of experiments in order to fully compare the newly proposed techniques with N3. We first set the degree of the polynomial model for all testing techniques to the one used in the simulation of bias field in the image, with the results illustrated in Fig. 4. We then run all techniques by fixing the degree of polynomial model in the estimation process for all images, with the results shown in Fig. 5. The Root Mean Squared Error (RMSE) statistics between the estimations and the ground truth used to measure the estimation accuracies.

We have several findings from the error statistics in Fig. 4 and Fig. 5. First, when a correct degree of the polynomial model is provided, N3 and our IRLS algorithm perform similarly but both worse than our linear programming technique, especially for a large degree value. Second, when the correct degree of polynomial model is unknown and the user needs to guess it, N3 deteriorates very quickly no matter the degree is set too high or too low, and in contrast the proposed techniques can produce accurate results if only a

¹<http://www.bic.mni.mcgill.ca/brainweb/>

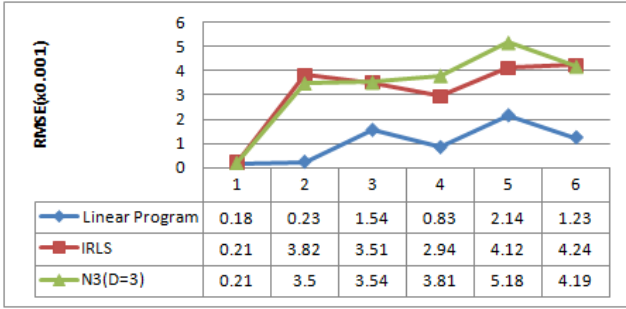


Figure 4. RMSE error statistics of bias field estimations on the six brain images in Fig. 3 with our techniques of solving a linear program and solving an IRLS, respectively, and N3 [10]. In these experiments, same degree of the polynomial model to the simulation is set for all techniques.

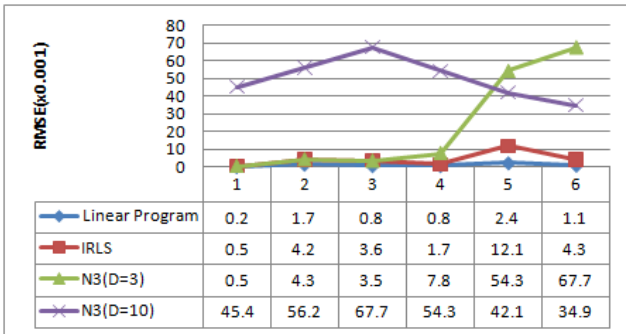


Figure 5. RMSE error statistics of bias field estimations on the six brain images in Fig. 3 with our techniques of solving a linear program and solving an IRLS, and with N3. For our techniques, the degree of the polynomial model is set to $D = 10$ in the estimation process. For N3, we set $D = 3$ and $D = 10$ respectively.

large enough degree is set (e.g. $D = 10$ in Fig. 5). N3 is incapable of adaptively determining the smoothness of the fit polynomial model, and the user needs to approximate it before running the algorithm. As shown in Fig. 5, when $D = 3$, N3 can estimate all simple bias fields accurately but deteriorates very quickly for more complex bias effects. It is because the degree is too low to accurately represent a very complicated bias field, as shown by the upper row of Fig. 6. When $D = 10$, estimations of N3 show obvious errors for all images. It is because that D is large enough to model the brain structure in the image. As a result, the bias field is over-estimated and brain structures can be seen in the estimated bias field, as shown by the lower row in Fig. 6. In contrast, our approaches can adaptively determine the complexity of bias field in a given image and produce high accuracies although the same D value is set, especially for the linear programming technique.

6.2. With Real Data

We also test our algorithms on 150 real brain images selected from 30 MRI T1 data sets in 3D, and compare the

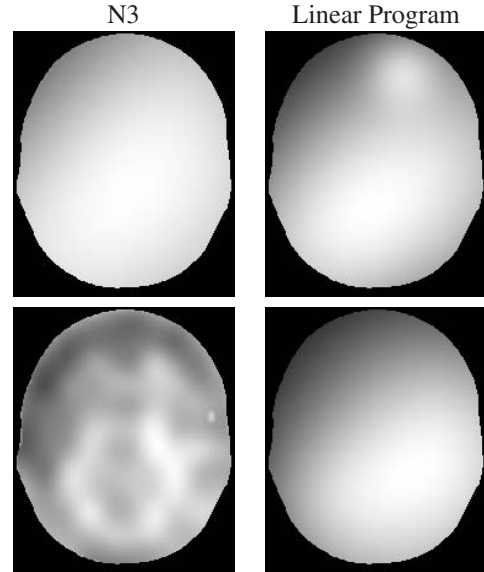


Figure 6. Bias field estimations. Left: results by N3. Right: results by our linear programming technique. Upper: results on the 6th brain image in Fig. 3. Lower: results on the 4th brain image in Fig. 3. N3 needs the user to manually set the smoothness degree of the bias field. When it is set too low ($D = 3$ for the upper row), under-estimation happens. If it is set too high ($D = 10$ for the lower row), over-estimation takes place. In contrast, our approach can adaptively determine an optimal smoothness degree.

accuracies with the original N3 technique² by visual evaluations and qualitative comparisons. For our approaches, we keep the parameter settings as explained above. For N3, we use the default parameter settings in the software, for which the distance between closest control points is 60.333mm. The 3D MRI volumes are all in size of $192 \times 256 \times 160$ and precision of $0.97 \times 0.97 \times 1.0 \text{ mm}^3$.

We obtain much better visual evaluations with our approaches than N3. For the 150 test images, we find 47 images with under-estimations by N3. For these images, bias fields estimated at the second time all show variation in magnitude by over 5% within the brain volume. There are also 3 images with obvious over-estimations. In contrast, we find only 2 images for which our IRLS algorithm produced under-estimations. No over-estimation is found for our two techniques, and no under-estimation is either found for our linear programming algorithm.

To quantitatively measure the accuracies of N3 and our approaches, we employ the coefficient of variation (COV) [10] to measure the intensity inhomogeneity in the white matter region. COV is the ratio between intensity variance and intensity mean value. A smaller COV value generally means a better correction of bias. We manually delineate the white matter regions for all the test images. For N3, our linear programming algorithm, and our IRLS algorithm, the

²<http://www.bic.mni.mcgill.ca/ServicesSoftware/HomePage>

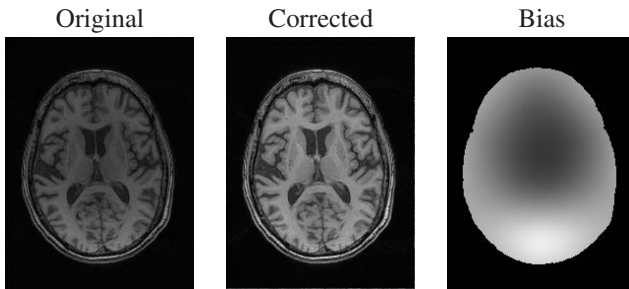


Figure 7. Bias field estimation result by the proposed techniques on a real MR brain image.

mean COV values over the 150 images are 6.3%, 1.5%, and 2.7%, respectively. It means that our approaches produce much better results. The estimated bias field for one example image by our IRLS method is shown in Fig. 7.

7. Conclusion

We propose a new scheme for image bias field estimation with two sparsity constraints. These two constraints enforce sparse representation on the corresponding bias-free image and the estimated bias field, respectively. They enable a solution by more efficient techniques and result in techniques with better performances than many previous methods.

Compared with previous methods, besides the multiple advantages listed in the main paper, another good property of our scheme is that it needs much fewer parameters to adjust by the user. In practice, our approach can mostly produce good results with the suggested values of λ and D in Sec. 6, and therefore the user doesn't need any adjustment at all. In contrast, many previous methods like N3 [10] require adjustments of multiple parameters. Adjusting multiple parameters needs some manual work like combinatorial optimization, and is usually a very hard task.

One weakness of our approaches is the possible confusion between the smooth changes of bias field and the intra-object intensity variations as explained in Sec. 1. We believe that few previous work can handle it due to its hardship.

We would expect to see better performances of our scheme by the following extensions. *First*, other image transformations (e.g. the wavelet transformation) are worthy to try to replace the simple image gradients. Total variation used in this paper suits to a piecewise constant image, and can not produce good result when the piecewise constancy doesn't hold. With other image transformations, better results are hopeful to be seen for even more complicated images (e.g. a highly textured image). *Second*, our scheme may produce better results with other models of bias field. For example, the piecewise polynomial model seems better suitable for illumination in indoor images and some outdoor images [11], and a radially symmetric model fits better the vignetting effect [15]. *Third*, we can try to sample a small portion of pixels and feed them to our linear programming

algorithm. Considering the smoothness of bias field, a good estimation can hopefully be produced while the speed is increased obviously. *Fourth*, we are eager to see the performances of our scheme on 3D medical data sets.

ACKNOWLEDGEMENT

The authors gratefully acknowledge NIH support of this work via grants EB006266, DA022807, NS045839, and NS065347.

References

- [1] S. Boyd and L. Vandenberghe. *Convex Optimization*. Cambridge University Press, 2004.
- [2] E. J. Candes and T. Tao. Decoding by linear programming. *IEEE Transactions on Information Theory*, 51:4203–4215, 2005.
- [3] E. J. Candes, M. B. Wakin, and S. P. Boyd. Enhancing sparsity by reweighted l1 minimization. *Journal of Fourier Analysis and Applications*, 14:877–905, 1999.
- [4] T. F. Chan and J. Shen. *Image Processing and Analysis - Variational, PDE, Wavelet, and Stochastic Methods*. SIAM, 2005.
- [5] D. L. Donoho. Compressed sensing. Technical report, Department of Statistics, Stanford University, 2004.
- [6] D. L. Donoho and X. Huo. Uncertainty principles and ideal atomic decomposition. *IEEE Transactions on Information Theory*, 47:2845–2862, 2001.
- [7] N. R. Draper and H. Smith. *Applied Regression Analysis*. John Wiley, New York, 2nd edition, 1981.
- [8] Y. Matsushita, S. Lin, S. B. Kang, and H.-Y. Shum. Estimating intrinsic images from image sequences with biased illumination. In *ECCV*, pages 274–286, 2004.
- [9] P. Meer. *Robust techniques for computer vision*, pages 107–190. Prentice-Hall, 2005.
- [10] J. G. Sled. *A nonparametric method for automatic correction of intensity nonuniformity in MRI data*. PhD thesis, GcGill University, May 1997.
- [11] M. F. Tappen, W. T. Freeman, and E. H. Adelson. Recovering intrinsic images from a single image. *IEEE Transactions on Pattern Recognition and Machine Intelligence*, 27(9):1459–1472, 2005.
- [12] G. Teschke and R. Ramlau. An iterative algorithm for nonlinear inverse problems with joint sparsity constraints in vector-valued regimes and an application to color image inpainting. *Inverse Problems*, 23:1851–1870, 2007.
- [13] U. Vovk, F. Pernus, and B. Lika. A review of methods for correction of intensity inhomogeneity in MRI. *IEEE Transactions on Medical Imaging*, 26(3):405–421, 2007.
- [14] Y. Zheng, S. Lin, C. Kambhamettu, J. Yu, and S. B. Kang. Single-image vignetting correction. *IEEE Transactions on Pattern Analysis and Machine Intelligence*, 31(12):2243–2256, 2009.
- [15] Y. Zheng, J. Yu, S. B. Kang, S. Lin, and C. Kambhamettu. Single-image vignetting correction using radial gradient symmetry. In *CVPR08*, 2008.